

# Laser-Calibrated System for Transnasal Fiberoptic Laryngeal High-Speed Videoendoscopy

\*Dimitar D. Deliyski, †Milen Shishkov, ‡§||Daryush D. Mehta, \*¶Hamzeh Ghasemzadeh, †Brett Bouma, #Matias Zañartu, \*\*Alessandro de Alarcon, and ‡§||Robert E. Hillman, \*¶East Lansing, Michigan, †‡§||Boston, Massachusetts, #Valparaiso, Chile, and \*\*Cincinnati, Ohio

**Summary:** The design specifications and experimental characteristics of a newly developed laser-projection transnasal flexible endoscope coupled with a high-speed videoendoscopy system are provided. The hardware and software design of the proposed system benefits from the combination of structured green light projection and laser triangulation techniques, which provide the capability of calibrated absolute measurements of the laryngeal structures along the horizontal and vertical planes during phonation. Visual inspection of *in vivo* acquired images demonstrated sharp contrast between laser points and background, confirming successful design of the system. Objective analyses were carried out for assessing the irradiance of the system and the penetration of the green laser light into the red and blue channels in the recorded images. The analysis showed that the system has irradiance of 372 W/m<sup>2</sup> at a working distance of 20 mm, which is well within the safety limits, indicating minimal risk of usage of the device on human subjects. Additionally, the color penetration analysis showed that, with probability of 90%, the ratio of contamination of the red channel from the green laser light is less than 0.002. This indicates minimal effect of the laser projection on the measurements performed on the red data channel, making the system applicable for calibrated 3D spatial-temporal segmentation and data-driven subject-specific modeling, which is important for further advancing voice science and clinical voice assessment.

**Key Words:** Vocal fold vibration—High-speed videoendoscopy—Laser calibration—Flexible endoscopy—Spatial calibrated measurements.

## INTRODUCTION

Vocal fold vibration during voice production is characterized by complex, three-dimensional (3D) kinematic patterns.<sup>1,2</sup> However, the *in vivo* quantitative analysis of these vibratory patterns requires the ability to perform absolute measurements of the length of the vocal folds, the amplitude of vibration, and different velocity measurements in calibrated units. Endoscopic laryngeal imaging techniques typically provide only a two-dimensional superior view of the vocal folds. They lack important information regarding the 3D vibratory patterns and do not provide absolute measurement of the

laryngeal tissues due to arbitrary zooming. To overcome this limitation, earlier attempts have been made to use the pixel intensity for estimating the 3D surface of the vibrating vocal folds.<sup>3</sup> However, since laryngeal tissues are not homogenous, their various structures have dissimilar reflection properties. Furthermore, the angle between different structures of the target surface and the imaging axis constantly changes during phonation. Hence, the intensity that is reflected back toward the camera also changes. Consequently, the intensity of pixels is a complex, and possibly nonlinear, function of distance to the endoscopic tip, the projection angle, and the reflection properties of tissues. Thus, the intensity of pixels only provides a rough estimation of the distance between the endoscopic tip and the target surface. Further complicated is the measurement of the size of objects from endoscopic images. One possible solution is adding fiducial markers with known topological properties to the field of view (FOV); then, recording the target surface with the superimposed fiducial markers simultaneously. For example, during laryngeal surgery, intraoperative measurements are performed by inserting a surgical instrument with a miniaturized ruler and using it as a scale for measuring the length of the adjacent tissues from the recorded images.<sup>4,5</sup> This approach has limited application outside the operating room where noninvasive fiducial markers are preferred.

Laser sources emit spatially coherent light, making them ideal candidates for creating patterns with specific and known topologies. In addition, their wavelength can be adjusted for optimal detection and minimal interference across color image channels (ie, red, green, and blue channels). These features make lasers an ideal candidate for creating noninvasive fiducial markers, which is one of the main

Accepted for publication July 16, 2019.

Portions of this study were presented at the 47th Symposium of The Voice Foundation: Care of the Professional Voice, Philadelphia, PA, USA, May 30 – June 03, 2018 and the 13th International Conference on Advances in Quantitative Laryngology, Voice and Speech Research, Montreal, QC, Canada, June 2 – 4, 2019.

Funding was provided by the Voice Health Institute, the Michigan State University Foundation, the National Institutes of Health – National Institute on Deafness and Other Communication Disorders (Grant number P50 DC015446), and the Comisión Nacional de Investigación Científica y Tecnológica, Chile (BASAL grant number FB0008). The content is solely the responsibility of the authors and does not necessarily represent the official views of the National Institutes of Health.

From the \*Department of Communicative Sciences and Disorders, Michigan State University, East Lansing, Michigan; †Wellman Center for Photomedicine, Massachusetts General Hospital, Harvard Medical School, Boston, Massachusetts; ‡Center for Laryngeal Surgery and Voice Rehabilitation, Massachusetts General Hospital, Boston, Massachusetts; §Department of Surgery, Harvard Medical School, Boston, Massachusetts; ||Division of Medical Sciences, Speech and Hearing Bioscience and Technology, Harvard Medical School, Boston, Massachusetts; ¶Department of Computational Mathematics Science and Engineering, Michigan State University, East Lansing, Michigan; #Department of Electronic Engineering, Universidad Técnica Federico Santa María, Valparaíso, Chile; and the \*\*Division of Pediatric Otolaryngology, Cincinnati Children's Hospital Medical Center, Cincinnati, Ohio.

Address correspondence and reprint requests to Dimitar D. Deliyski, Michigan State University, Department of Communicative Sciences and Disorders, 1026 Red Cedar Road, Oyer Speech & Hearing, East Lansing, MI 48824-1220.  
E-mail: [ddd@msu.edu](mailto:ddd@msu.edu)

Journal of Voice, Vol. 35, No. 1, pp. 122–128  
0892-1997

© 2019 The Voice Foundation. Published by Elsevier Inc. All rights reserved.  
<https://doi.org/10.1016/j.jvoice.2019.07.013>

reasons for their usage in laryngeal imaging systems with calibrated measurements and/or 3D reconstruction capabilities.<sup>6</sup> The approaches for creating the laser fiducial markers include the triangulation technique, structured light projection, or their combination. In the laser triangulation technique, the angle difference between the imaging axis and the laser projection beams encodes the vertical displacements<sup>7</sup> in such a way that the position of laser points on a set of deterministic trajectories can be used for measuring the vertical distances.<sup>8</sup> Figure 1A depicts the projection of a single laser point on two imaginary surfaces, S1 and S2, that have a vertical difference of  $h$ . The movement of the laser point from S1 to S2 leads to a horizontal displacement in the FOV ( $\Delta$ ) that is reflected on the camera sensor chip as a displacement ( $\delta$ ) in the captured digital image. In that,  $\Delta$  and  $\delta$  are linearly related as a function of the magnification factor of the camera ( $m$ ). The relationship between  $h$ ,  $\Delta$ , and the angle between the imaging and the projection axes ( $\theta$ ) is governed by trigonometric laws. The vertical displacement can be measured using Equation 1, as follows:

$$h = \frac{\delta}{m \cdot \tan \theta} \quad (1)$$

Single-point<sup>9</sup> and single-line<sup>10</sup> laser projection systems are examples that have used the triangulation technique. On the other hand, in structured light projection, usually a set of parallel beams with a known distance ( $d$ ) from each other are projected on the target surface. Because the distance between the parallel lines does not change, their positions on the recorded image can be used as a ruler for converting the horizontal distances on the image into units of absolute physical distance (eg, millimeters). Figure 1B shows a simple schematic of this technique. A few systems used structured light projection for achieving calibrated measurements.<sup>4,11,12</sup> Finally, it is possible to combine the two techniques for making measurements along the horizontal and vertical planes simultaneously. Figure 1C shows a simple schematic of this technique. In this fashion, a set of laser beams (or lines) with known topology are projected on the target surface.

Therefore, laser triangulation can be used on each laser points for finding the vertical distance. More specifically, the changes in vertical distance result in specific direction and magnitude of displacement ( $D$ ) for the pattern.<sup>8</sup> Additionally, the pairwise distances between laser points ( $d_1, d_2$ ) can be used as a ruler for making horizontal measurements. The multiple laser point projection<sup>8,13–15</sup> and multiple parallel line projection<sup>16</sup> approaches are examples of systems that have used the combination of both techniques.

This paper presents the first system capable of performing laser-calibrated transnasal flexible endoscopy compatible with laryngeal high-speed videoendoscopy (HSV). Previous state-of-the-art systems were either: (1) capable of HSV-compatible transnasal flexible endoscopy without calibration<sup>17,18</sup>; (2) capable of HSV-compatible laser-calibrated measurement only with rigid endoscopy<sup>6,9–11,14–16</sup>; or (3) capable of laser-calibrated transnasal flexible videostroboscopy, noncompatible with HSV.<sup>13</sup> The main advantages of the new system are threefold. First, the hardware (optics) and software (algorithms) design benefits from the combination of structured light projection and laser triangulation techniques, providing calibrated measurement capabilities on both, horizontal and vertical planes, making 3D surface reconstruction of vocal fold vibration possible. Second, the hardware and software aspects of the system are designed to comply with specific characteristics and requirements of flexible endoscopy. Therefore, the system could be used to study and elicit a wide range of stimuli and laryngeal configurations and functions including studying complex laryngeal maneuvers and connected speech. Third, the hardware and software aspects of the system were designed to be operable with HSV, giving the system capability of capturing fast, transient and nonperiodic phenomena that are inherent to production of connected speech but cannot be captured by videostroboscopy.<sup>5,19</sup>

## HARDWARE DESIGN AND SPECIFICATION

The laser-calibrated endoscopic system was designed by upgrading existing surgical fiberoptic endoscopes. The

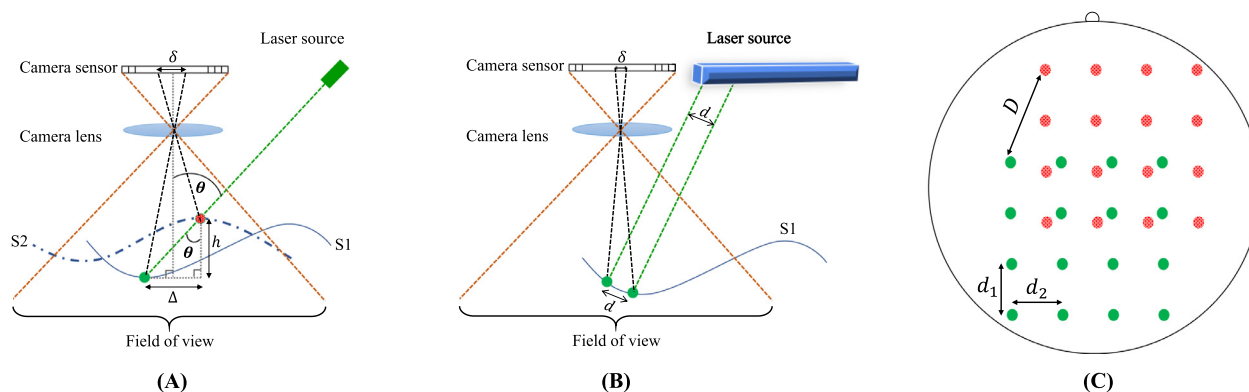


**FIGURE 1.** Schematics of laser projection techniques with the principle of encoding the vertical and/or horizontal distances using: A. laser triangulation method; B. structured light projection; and C. a combined technique. The green (solid) and red (patterned) dots depict hypothetical positions of the laser pattern at two different vertical distances. (For interpretation of the references to color in this figure legend, the reader is referred to the Web version of this article.)

adult version of the laser-calibrated endoscope utilized the Fiber Naso Pharyngo Laryngoscope Model FNL-15RP3 (PENTAX Medical, Montvale, NJ). This endoscope has an insertion tube diameter of 4.9 mm, surgical instrument channel diameter of 2.1 mm, working length of 300 mm, and a 75° angle of view. The pediatric version was based on the Rhino Laryngo Fiberscope Model 11001RD (KARL STORZ Endoscopy-America, Inc., El Segundo, CA). This endoscope has insertion tube diameter of 3.5 mm, surgical instrument channel diameter of 1.5 mm, working length of 340 mm, and a 90° angle of view. The choice of surgical endoscopes was made because the surgical channel provides the most convenient mechanism for accommodating internally the laser-projection system allowing to project the laser patterns onto the FOV using commercially available endoscopes. Additionally, the optical imaging channel, the laser-projection fiber, and the light-delivering channel are bundled together and sealed, allowing disinfection. Finally, the selected endoscopes allow sufficient brightness of the light-delivering channel and the optical image necessary to warrant HSV speeds of at least 4,000 frames per second (fps).

Figure 2 shows the distal end of the adult endoscope with its corresponding channels. The distal end of endoscope is the terminal of the three main channels. The surgical instrument channel incorporates a diffraction-based laser projection system for projecting the desired laser pattern on the FOV. The output window of the laser projector was sealed with ultra violet curing epoxy. The projector was glued in the tilting fixture for the adult scopes with 5-minute epoxy. The tilting fixture for the adult projector and the pediatric projector we sealed in the instrument channels with Dow Corning 748 silicone sealer. The optical imaging channel is coupled to a high-speed digital camera for recording of the FOV superimposed with the projected laser pattern. The third channel can be attached

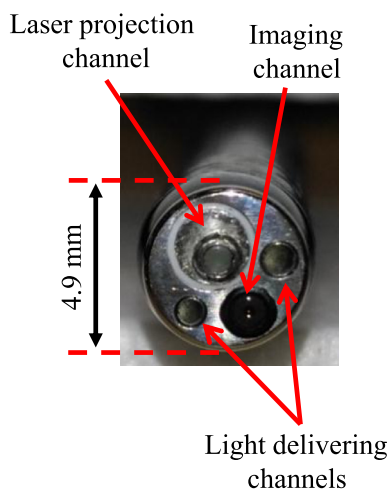


**FIGURE 2.** Distal end of the adult endoscope showing the terminals of the three types of channels of the system: the laser-projection, the light-delivery and the optical imaging channels.

to a xenon light source with power up to 300 W for delivering light to the target surface.

The laser-projection system is designed based on a combination of triangulation technique and structured light projection. This design allows for performing calibrated measurements on both horizontal and vertical planes, as well as capturing the kinematic and 3D representations of the vocal fold vibratory patterns. The laser-projection system used a green-laser light with wavelength of 520 nm. This wavelength was selected as a trade-off between maximizing the detection probability of laser points in the green channel of the image and minimizing the interference into the red channel for data collection purposes. The laser beam is guided through the surgical channel using an optical fiber and is divided into a mesh pattern of  $7 \times 7$  green laser points, creating a square of  $16 \times 16$  mm at a working distance of 20 mm. The structured laser pattern is projected on the FOV and it provides the necessary information for calibrating the measurements on the horizontal plane. Figure 3A shows the details of the designed probe. The fiber optic (FO) probe consists of an external part I and an internal part II. Externally mounted to the endoscope is a Luer-lock tip connecting to the instrumental channel port and holding the FO cable with a Diamond E2000 connector (Diamond SA, Losone, Switzerland) at the proximal end and two stress-relieve boots at both ends of the FO cable. The internal part of the probe consists of a buffered optical fiber and the distal optics residing in a sealed capsule. Figure 3B shows the details of the optical design at distal end of the probe for creating the grid pattern from the laser beam. The distal optics are based on a diffractive optical element (DOE) made by HOLOEYE Photonics AG (Berlin-Adlershof, Germany). A dot-matrix beam splitter produces a  $7 \times 7$  dot matrix. The beam from the optical fiber is collimated by a gradient-index (GRIN) lens. The DOE is cemented to the output surface of the GRIN lens with its pattern facing out. The whole assembly is encapsulated in a titanium body. The pattern is projected on the tissue through a sapphire window that is sealed to the body allowing sterilization and cleaning, and protecting the DOE pattern. The Dot pattern is centered in the FOV by tilting the body toward the objective in the adult laryngoscopes or by displacing the fiber off the optical axis in the pediatric laryngoscopes.

The laser source is a 520-nm diode laser from Blue Sky Research (Milpitas, CA). A custom power supply and control box was developed for the laser source. External AC-to-DC 24-V medical grade adapter powers the box via power input socket. A key switch powers the main board and an indicator diode shows its status (on/off). The output power of the laser is controlled by a potentiometer and displayed in units of mW (approximate power of the dot pattern) on an indicator. The laser light is supplied by smf-28 multi-mode (in 520 nm) fiber from the laser diode to the output adapter, where it is connected to the Diamond E2000 connector. Figure 4 depicts the finalized system with its different components.

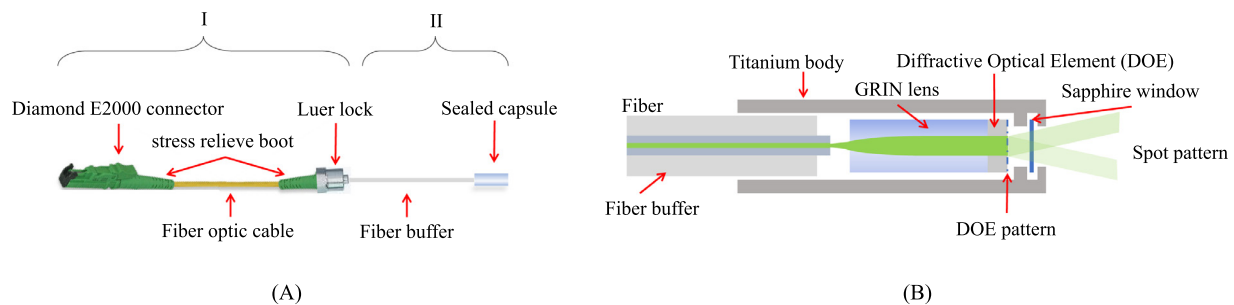


**FIGURE 3.** Structured-pattern laser projection: A. schematic of the designed probe; B. diffraction method for splitting the laser beam into the desired pattern.

## RESULTS AND ANALYSIS

### Visual assessment of laser points contrast

The functionality of the system and visibility of the laser patterns were evaluated subjectively using a single male subject. The reason for testing the system on a male subject was that male larynges are deeper, creating challenges with image brightness; thus, if the system performed well at longer distances and darker images, it would create less issue with female subjects. The eyepiece of the endoscope was coupled to a color Phantom Miro LC310 high-speed camera (Vision Research Inc., Wayne, NJ) recording the FOV at the rate of 6,000 fps. The light-delivery channel of the endoscope was connected to a 300-W xenon light source (Model 7152A, PENTAX Medical, Montvale, NJ), and all recordings were carried out at full illumination. The subject was asked to perform a series of pitch glides. Each time, the endoscope was subjectively positioned at different vertical distances from the vocal folds, providing close-up, mid-distance, and further-distance views of the vocal folds. Figure 5 shows example frames from each of those recordings. The visibility of the laser patterns in the FOV was clear, demonstrating the successful development of the laser-projection system.

### Laser points average power and irradiance

The laser-projection system utilized a 45-mW laser source for creating the projected pattern. The laser power was measured to be up to 20 mW at the distal end of the endoscope when the laser source is set at full power (the unit allows manually varying the output power from 0 to 20 mW). Additionally, in order to compute the amount of irradiance, the areas of laser points at different working distances were measured. Using the protocol described in Ghasemzadeh et al,<sup>8</sup> two different sets of recordings were made using a monochrome high-speed camera Phantom v7.1 (Vision Research Inc.). In the first set, the xenon light was turned on, the laser source was turned off and a multiresolution grid paper (1-mm, 2-mm, and 10-mm boxes) was recorded at working distances of 15 mm, 20 mm, and 25 mm. The diameter of the FOV was measured from these recording, and then the diameter was used as a scale for converting from pixels into millimeters for that working distance. In the second set, the xenon light was turned off, the laser source was turned on, and a white paper was recorded at working distances of 15 mm, 20 mm, and 25 mm.

The following approach was used for segmentation of the laser points from each recording. To remove the effect of

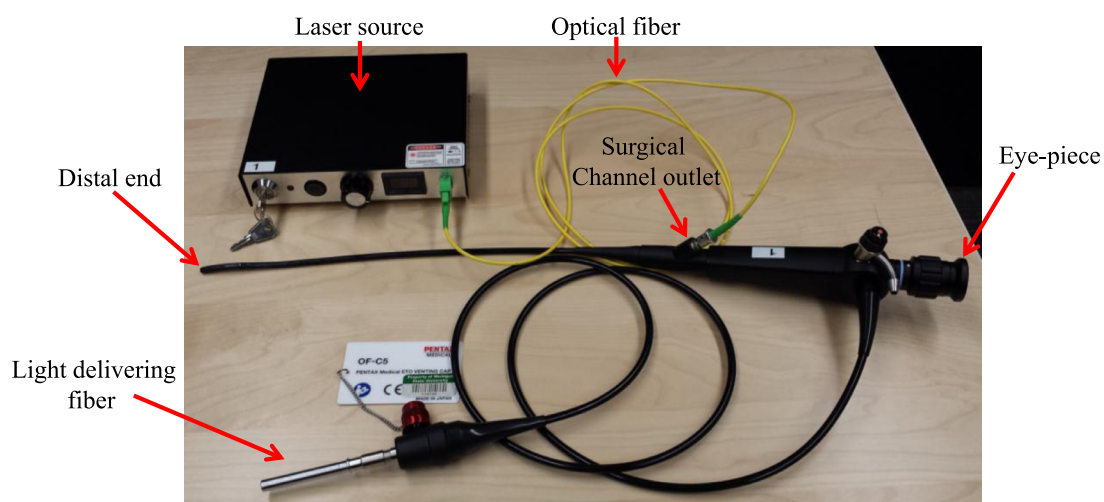


**FIGURE 4.** The main components of the laser-calibrated system for laryngeal transnasal fiberoptic HSV imaging. HSV, high-speed video-endoscopy.

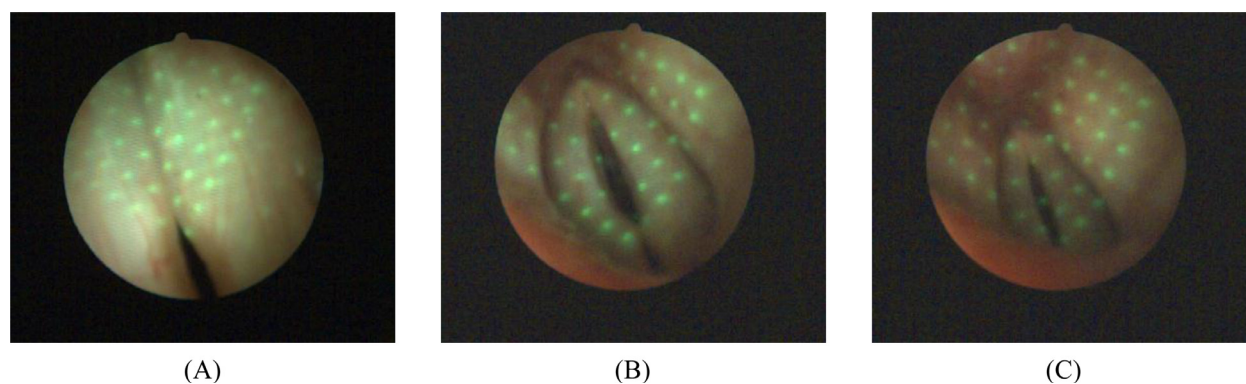


**FIGURE 5.** Examples of single frames from the *in-vivo* high-speed videoendoscopic recordings during phonation using the laser-projection system during full xenon-light exposure: A. close-up view; B. mid-distance view; and C. further-distance view.

additive noise, all frames were averaged, and the histogram of pixel intensities was computed using 200 bins. Pixels that fell in the first bin were considered as the black reference and were discarded. The histogram of the logarithms of the remaining pixel intensities was constructed. The segmentation threshold was computed from this histogram such that the segmented image kept at least 80% of the energy of the original image. Based on this approach, the number of pixels in each laser point was counted, and then the area of each laser point was converted into millimeters using the estimated scale from the corresponding recording from the first set. [Table 1](#) reports the descriptive statistics of the areas from different laser points. Additionally, assuming a uniform distribution of the laser power over the area and no loss during the transmission, the irradiance was computed by dividing the laser power at the distal end of the endoscope by the summation of the areas from all the laser points. [Table 1](#) also presents the estimated irradiance at different working distances. As shown, the irradiance varies from 262 to 389 W/m<sup>2</sup> at working distances from 25 to 15 mm. This is well within the acceptable safety limits of 11,000 W/m<sup>2</sup> for short exposures of 1 second and 2,000 W/m<sup>2</sup> for long exposures above 10 seconds, indicating minimal risk of usage of the device on human subjects for any exposure.<sup>6,20</sup>

### Green-laser penetration into the red and blue color channels

Previous studies have shown that the red channel carries most of the necessary information for segmentation and

quantitative measurements of vocal fold vibration.<sup>21</sup> Therefore, it is very important that the red channel contamination from the laser source be as minimum as possible. An estimation of the leakage of energy from the green laser into the red channel could provide that information. At the same time, leakage of laser energy into other color channels could provide an estimate of efficiency of the system. That is, in the ideal case we would like the laser light to be only present in the green channel. In that case, the energy would be distributed over a smaller spectral bandwidth, and hence the laser points on the image would have higher energy and sharper contrast. Therefore, we could achieve higher detection rate or instead reduce the power of the laser source for achieving the same level of accuracy.

To find the leakage of green laser into the other color channels, a set of experiments was carried out in a dark environment and with the xenon light source turned off. The laser points were projected on a white piece of paper at a working distance of 20 mm. The FOV was recorded using a color high-speed camera (Phantom Miro LC310) at the rate of 6,000 fps, and results were stored in raw (pre-Bayer-decoding) format. During the data collection, specific attention was placed on the brightest laser points to ensure that no pixels were saturated. In case of such instances, the exposure time of the camera was reduced. The raw data before any color interpolation was then imported into MATLAB for further analysis. In the analysis, the three-color channels were separated, and the laser points were segmented in the green channel using the exact same procedure in the previous section. Then, the computed mask from the green channel was applied to the red and the blue channels, and the ratio of value of pixels in red to green (Red/Green) and the ratio of value of pixels in blue to green (Blue/Green) were determined. The same procedure was repeated for different laser powers. The distribution of the resulting ratios when the power of laser was 20 mW is presented in [Figure 6](#). To assist with the interpretation, [Table 2](#) reflects different percentiles of distribution for Red/Green and Blue/Green ratios when the power of laser source was varied.

Referring to [Figure 6](#), the distribution of leakage into the red channel (the channel used for segmentation and measurement) has very sharp peak around a very small number,

**TABLE 1.**  
Area of Laser Points and Irradiance at Different Working Distances

Working Distance (mm)	Area (mm <sup>2</sup> )		Irradiance (W/m <sup>2</sup> )
	mean	std	
15	10.5	3.6	389
20	11	5.3	372
25	15.2	8.4	262

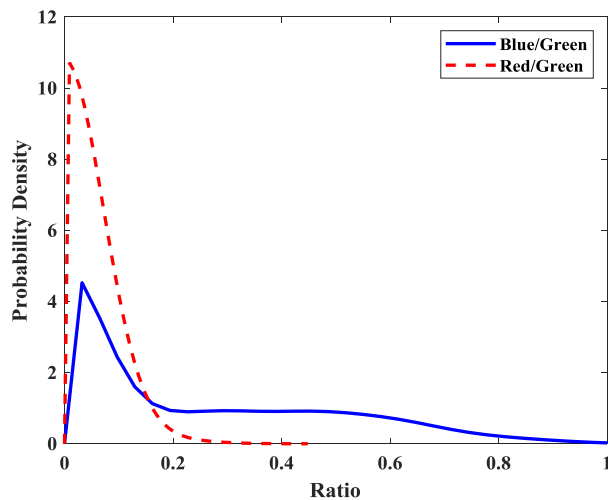


**FIGURE 6.** Probability density functions of Red/Green (*dashed line*) and Blue/Green (*solid line*) ratios when laser power is 20 mW. (For interpretation of the references to color in this figure legend, the reader is referred to the Web version of this article.)

this characteristic indicates that the laser points do not add significant contamination to the red channel. This characteristic becomes clearer by looking at Table 2, which shows that, with probability of 70%, the ratio of contamination is less than  $10^{-4}$ , and with probability of 90%, the ratio of contamination is less than 0.002. For the Blue/Green ratio, a different trend is seen. Figure 6 shows a highly dispersed distribution that could go even above 0.8. In addition, more quantitative results can be inferred from Table 2. When the laser is at full power, with probability of 10%, the amount of contamination of the blue channel reached as high as 0.613. Therefore, we could conclude that a significant amount of green energy from the laser leaked into the blue channel. Further investigation into the spectral response of the camera sensor can help with the interpretation of these observations. The spectral response of the sensor at the wavelength of 520 nm shows curves for the blue and green sensors with relatively high values, indicating large pixel-intensity values in both blue and green channel for the laser points. On the other hand, the curve for the red sensor has

very small value, indicating very small pixel values in the red channel for the laser points. The camera manufacturer's (Vision Research Inc.) specifications confirm and explain these experimental results.

## CONCLUSION

The proposed transnasal laryngeal high-speed videoendoscopy system provides the capability of absolute measurements from *in vivo* recordings in both horizontal and vertical planes. The subjective visual assessment of the recordings showed visible and sharp contrast between the laser points and the background, confirming successful design of the system. Additionally, low leakage of the green laser light into the red channel warrants low contamination of data acquisition and measurement from the red channel. Future work calls for the development of a vertical and horizontal calibration protocol and custom image-processing software for automated calibrated measurements in the application of the laser-calibrated system for transnasal laryngeal fiberoptic high-speed videoendoscopy.

## SUPPLEMENTARY MATERIALS

Supplementary material associated with this article can be found in the online version at <https://doi.org/10.1016/j.jvoice.2019.07.013>.

## REFERENCES

- Moore P, Von Leden H. Dynamic variations of the vibratory pattern in the normal larynx. *Folia Phoniatr Logop.* 1958;10:205–238.
- Hunter EJ, Titze IR, Alipour F. A three-dimensional model of vocal fold abduction/adduction. *J Acoust Soc Am.* 2004;115:1747–1759.
- Shaw HS, Deliyski DD. Vertical motion during modal and pressed phonation: magnitude and symmetry. In: Manfredi C, ed. In: *Proceedings of the Fourth International Workshop on Models and Analysis of Vocal Emissions for Biomedical Applications*. Firenze, Italy: Firenze University Press; 2005;4:133-136.
- Schade G, Leuwer R, Kraas M, et al. Laryngeal morphometry with a new laser “clip on” device. *Lasers Surg Med Off J Am Soc Laser Med Surg.* 2004;34:363–367.
- Powell M, Deliyski D, Zeitels S, Burns J, Hillman R, Gerlach T MD. Efficacy of Videostroboscopy and High-Speed Videoendoscopy to Obtain Functional Outcomes From Perioperative Ratings in Patients With Vocal Fold Mass Lesions. *J Voice.* 2019. [Epub ahead of print]. <https://doi.org/10.1016/j.jvoice.2019.03.012>. PubMed PMID: 31005449.
- Semmler M, Döllinger M, Patel RR, et al. Clinical relevance of endoscopic three-dimensional imaging for quantitative assessment of phonation. *Laryngoscope.* 2018;128:2367–2374.
- Ji Z, Leu M-C. Design of optical triangulation devices. *Opt Laser Technol.* 1989;21:339–341.
- Ghasemzadeh H, Deliyski D, Ford D, et al. Method for vertical calibration of laser-projection transnasal fiberoptic high-speed videoendoscopy. *J Voice.* 2019. [Epub ahead of print]. <https://doi.org/10.1016/j.jvoice.2019.04.015>. PubMed PMID: 31151853.
- Larsson H, Hertegård S. Calibration of high-speed imaging by laser triangulation. *Logop Phoniatr Vocology.* 2004;29:154–161.
- George NA, de Mul FFM, Qiu Q, et al. New laryngoscope for quantitative high-speed imaging of human vocal folds vibration in the horizontal and vertical direction. *J Biomed Opt.* 2008;13:64024.
- Schuberth S, Hoppe U, Döllinger M, et al. High-precision measurement of the vocal fold length and vibratory amplitudes. *Laryngoscope.* 2002;112:1043–1049.

**TABLE 2.**

**Percentile of Leakage From Green Laser Light Into Red and Blue Channels for Different Laser Power Settings ( $\epsilon$  means  $<10^{-4}$ )**

Laser Power (mW)	Red/Green			Blue/Green		
	50%	70%	90%	50%	70%	90%
10	$\epsilon$	$\epsilon$	$\epsilon$	$\epsilon$	0.076	0.468
12	$\epsilon$	$\epsilon$	$\epsilon$	0.011	0.222	0.507
14	$\epsilon$	$\epsilon$	$\epsilon$	0.038	0.281	0.557
16	$\epsilon$	$\epsilon$	$\epsilon$	0.088	0.359	0.58
18	$\epsilon$	$\epsilon$	0.001	0.126	0.388	0.594
20	$\epsilon$	$\epsilon$	0.002	0.154	0.391	0.613

12. Hanson DG, D'Agostino MC USAF M, Jiang J, et al. Clinical measurement of mucosal wave velocity using simultaneous photoglottography and laryngostroboscopy. *Ann Otol Rhinol Laryngol*. 1995;104:340–349.
13. Kobler JB, Rosen DI, Burns JA, et al. Comparison of a flexible laryngoscope with calibrated sizing function to intraoperative measurements. *Ann Otol Rhinol Laryngol*. 2006;115:733–740.
14. Luegmair G, Mehta DD, Kobler JB, et al. Three-dimensional optical reconstruction of vocal fold kinematics using high-speed video with a laser projection system. *IEEE Trans Med Imaging*. 2015;34:2572–2582.
15. Luegmair G, Kniesburges S, Zimmermann M, et al. Optical reconstruction of high-speed surface dynamics in an uncontrollable environment. *IEEE Trans Med Imaging*. 2010;29:1979–1991.
16. Patel RR, Donohue KD, Lau D, et al. In vivo measurement of pediatric vocal fold motion using structured light laser projection. *J Voice*. 2013;27:463–472.
17. Zaňartu M, Mehta DD, Ho JC, et al. Observation and analysis of in vivo vocal fold tissue instabilities produced by nonlinear source-filter coupling: a case study. *J Acoust Soc Am*. 2011;129:326–339.
18. Mehta DD, Deliyski DD, Zeitels SM, et al. Integration of transnasal fiberoptic high-speed videoendoscopy with time-synchronized recordings of vocal function. In: Izdebski K, Yan Y, Ward RR, Wong B, Cruz RM, eds. *Normal & Abnormal Vocal Folds Kinematics: HSDP, OCT & NBI<sup>®</sup>, Volume I: Technology*. San Francisco: Pacific Voice & Speech Foundation; 2015:105–114.
19. Mehta DD, Hillman RE. Current role of stroboscopy in laryngeal imaging. *Curr Opin Otolaryngol Head Neck Surg*. 2012;20:429–436.
20. Semmler M, Kniesburges S, Parchent J, et al. Endoscopic laser-based 3D imaging for functional voice diagnostics. *Appl Sci*. 2017;7:600.e1-600.e18.
21. Naghibolhosseini M, Deliyski DD, Zacharias SRC, et al. Temporal segmentation for laryngeal high-speed videoendoscopy in connected speech. *J Voice*. 2018;32. 256.e1-256.e12.